Available online at www.sciencedirect.com
SCIENCE DIRECT
Journal of Power Sources 157 (2006) 522–527
JOURNAL OF POWER SOURCES
www.elsevier.com/locate/jpowsour

Short communication

$CuFe_2O_4/SnO_2$ nanocomposites as anodes for Li-ion batteries

R. Kalai Selvan [a,c], N. Kalaiselvi [a,*], C.O. Augustin [a], C.H. Doh [b], C. Sanjeeviraja [c]

[a] *Central Electrochemical Research Institute, Karaikudi 630006, India*
[b] *Korea Electrotechnology Research Institute, Changwon 641-120, Republic of Korea*
[c] *Department of Physics, Alagappa University, Karaikudi 630003, India*

Received 29 March 2005; accepted 15 July 2005
Available online 16 September 2005

Abstract

Ultrafine powders of nanocrystalline $CuFe_2O_4$ and $CuFe_2O_4$/10 wt.% SnO_2 nanocomposites are prepared by a urea–nitrate combustion method. Phase pure and highly crystalline $CuFe_2O_4$ (tetragonal structure) and $CuFe_2O_4/SnO_2$ (cubic structure) are obtained after sintering at 1100 °C. The average particle size is 10–20 and 20–30 nm, respectively. Both the nanoferrite anodes have an excellent specific capacity of greater than 800 mAh g^{-1} versus Li metal. It is concluded that SnO_2 doping improves the coulombic efficiency of copper ferrite anodes from 65 to 99.5% via an enhanced structural stability.

Keywords: Copper ferrite; Nanocomposites; Lithium-ion batteries; Specific capacity; Coulombic efficiency

1. Introduction

In recent years, a great deal of attention has been given to the development of energy devices for portable electronic applications. In particular, a tremendous amount of research is being conducted on lithium-ion battery technology to meet the varied requirements of consumer markets. Despite commercialization of Li-ion batteries, carbonaceous negative electrodes (anodes), which are known for their high capacity values, suffer from large irreversible capacity losses. As a result, there is an urgent need to identify suitable alternative materials to carbon/graphite. This has opened up new avenues for the deployment of transition metal oxides [1–3], metal–metal alloys [4–6], transition metal vanadates [7], ATCO anodes [8,9], metalloids [10], lithium metal oxides, such as $LiMSnO_4$ [11], phosphates [12], and niobates [13]. More recently, spinel-type ferrite anodes, viz. $CoFe_2O_4$ [14,15], $NiFe_2O_4$ [16,17], $ZnFe_2O_4$ [18], and $CaFe_2O_4$ [19] have gained in importance due to their high specific capacities and facile synthesis.

To date, there have been no reports on the possibility of employing $CuFe_2O_4/SnO_2$ nanocomposites as anode materials for Li-ion batteries. It is well known that SnO_2 displays excellent reversible properties when used as an anode, and can store twice the amount of Li^+ ions compared with graphite. Consequently, various forms of SnO_2 have been reported as lithium battery anodes [20–23]. The study reported here attempts to enhance the electrochemical activity of native $CuFe_2O_4$ through the incorporation of SnO_2.

In this respect, nanocrystalline $CuFe_2O_4$ and $CuFe_2O_4/SnO_2$ nanocomposites have been synthesized by means of a urea–nitrate combustion method. The investigation identifies the advantages of deployment of nanocomposite electrodes and the effect of SnO_2 dopant in reducing the Li^+ ion diffusion path lengths so as to enhance the diffusion kinetics and impart improved charge–discharge characteristics.

2. Experimental

2.1. Synthesis

Nanocrystalline $CuFe_2O_4$ and $CuFe_2O_4/SnO_2$ powders were prepared by means of a urea–nitrate combustion

* Corresponding author. Tel.: +91 4565 227550–9; fax: +91 4565 227713/79.
E-mail address: kalakanth2@yahoo.com (N. Kalaiselvi).

0378-7753/$ – see front matter © 2005 Elsevier B.V. All rights reserved.
doi:10.1016/j.jpowsour.2005.07.030

method. The synthesis procedure and thermodynamical calculations of the parent $CuFe_2O_4$ have been reported elsewhere [24]. The synthesis of composite ferrite ($CuFe_2O_4/SnO_2$) powder was performed as follows. Stoichiometric quantities of $Cu(NO_3)_2{\cdot}6H_2O$, $Fe(NO_3)_3{\cdot}9H_2O$, SnO_2, HNO_3, and $CO(NH_2)_2$ were dissolved in 100 ml of distilled water. The mixed nitrate–urea solution was heated at 110 °C, with continuous stirring. After the evaporation of excess of water, a highly viscous gel, known as the precursor, was obtained. The gel was ignited at 300 °C to remove the undesirable gaseous products, and form the desired product as a foamy powder. Finally, the powder was sintered at different temperatures, e.g., 800, 1000, and 1100 °C, for 5 h to obtain ultrafine powders of $CuFe_2O_4/SnO_2$ nanocomposites.

2.2. Characterization

The phase purity and crystallinity of the ferrite materials were identified by powder X-ray diffraction analysis with an X-ray diffractometer (Rigaku Dmax/2C, Japan with Cu Kα radiation; $\alpha = 1.5405$ Å). Surface morphology and particle size were analyzed by means of scanning electron microscopy (SEM; JEOL S-3000 Model) and transmission electron microscopy (TEM; JEOL-JEM 100SX microscope at an accelerating voltage of 200 kV), respectively. The specimens for TEM investigations were prepared by placing a drop of each sample suspension on a carbon-coated copper grid (400 mesh, Electron Microscopy Sciences) and allowing this to dry in air under ambient conditions.

2.3. Electrode fabrication

The negative (anode) electrode was prepared by coating a mixed slurry of synthesized ferrite powder (80 wt.%), VGCF (6 wt.%), SPM (6 wt.%), and PTFE binder (8 wt.%) over a copper foil of 10 μm in thickness. The powders were mixed thoroughly in the appropriate ratios and made in to a slurry by using NMP as solvent. The electrodes were hot rolled, punched into dimensions of 5 in. × 3 in., and stored in the dry room for at least 24 h prior to cell fabrication. The electrodes were evaluated against lithium foil of thickness 120 μm in an electrolyte of 1:1 (v/v) ethyl carbonate:diethyl carbonate dissolved in 1 M $LiPF_6$. A polypropylene separator (Asahi) of 20 μm thickness with 40% porosity was used. The fabricated pouch cells were aged in a dry room for 1 day and were then subjected to charge–discharge cycling [12].

3. Results and discussions

3.1. Structural analysis

The X-ray diffraction patterns recorded for $CuFe_2O_4$ and $CuFe_2O_4$/10 wt.% SnO_2 samples heat-treated at 300, 800, 1000, and 1100 °C are presented in Figs. 1 and 2. It is evident from XRD observations that a temperature of 300 °C is insufficient for the formation of $CuFe_2O_4$. Rather, a minimum of 800 °C is essential to obtain $CuFe_2O_4$ with a tetragonal structure and $CuFe_2O_4/SnO_2$ with a cubic structure. Although crystallization of the products is well initiated at 800 °C, improved crystallinity is expected at higher temperatures. This is because even at 800 °C, the intensity of the individual peaks is not optimum and is an indication of incomplete crystallinity (Figs. 1 and 2). Therefore, the powders were further sintered at higher temperatures, such as 1000 and 1100 °C. As expected, the product obtained after sintering at 1100 °C exhibits sharp and well-defined Bragg peaks with preferred intensity. Thus, the urea–nitrate combustion method can yield fine powders of $CuFe_2O_4$ and $CuFe_2O_4/SnO_2$ with a high degree of phase purity and crystallinity at high sintering temperatures. The absence of undesirable peaks ensures the phase purity of both the ferrite samples.

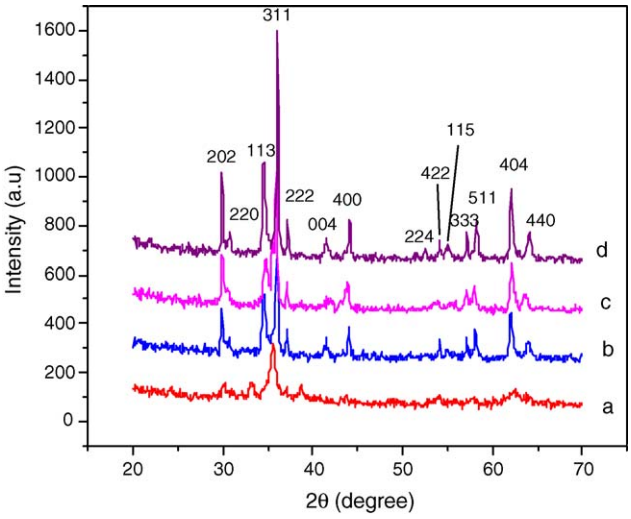

Fig. 1. XRD pattern of $CuFe_2O_4$ sintered at (a) 300 °C, (b) 800 °C, (c) 1000 °C, and (d) 1100 °C.

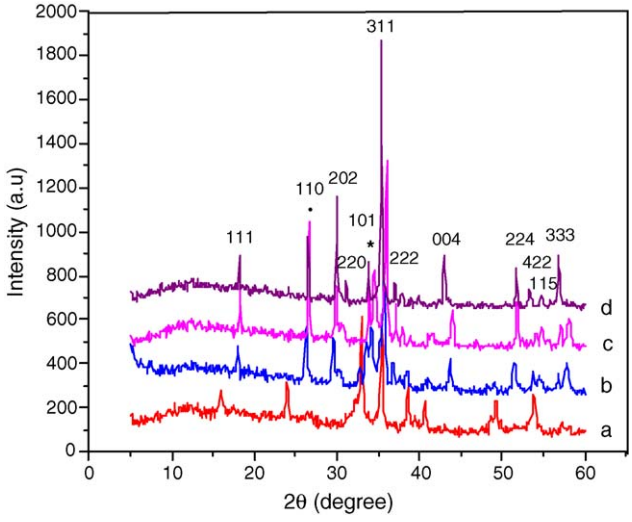

Fig. 2. XRD pattern of $CuFe_2O_4/SnO_2$ sintered at (a) 300 °C, (b) 800 °C, (c) 1000 °C, (d) 1100 °C. (*) SnO_2.

The XRD peaks of $CuFe_2O_4$ and $CuFe_2O_4/SnO_2$ were indexed, respectively, for tetragonal and cubic lattice patterns. Perfect matching with the standard values was obtained in both cases. Comparison of the lattice constant values of $CuFe_2O_4$ [$a = 8.274$ Å; $c = 8.4814$ Å] and $CuFe_2O_4/SnO_2$ [$a = 8.4082$ Å; $c = 8.3744$ Å] synthesised at 1100 °C shows that SnO_2 doping enhances lattice constants. This, in turn, is an indication that SnO_2 has been incorporated into the crystal lattice of the parent $CuFe_2O_4$ compound. In addition, the XRD pattern of $CuFe_2O_4/SnO_2$ contains peaks that are due to SnO_2 along with the peaks for $CuFe_2O_4$, and thus further confirms that doping of SnO_2 into the $CuFe_2O_4$ matrix has taken place.

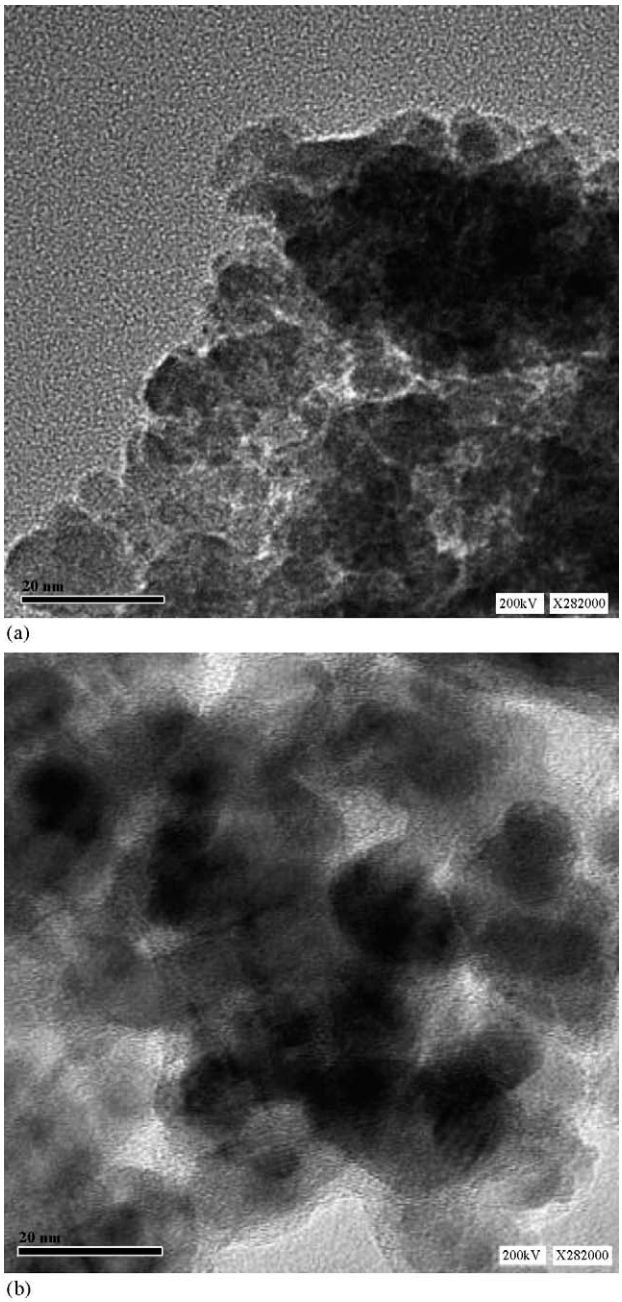

Fig. 3. TEM images of (a) $CuFe_2O_4$ and (b) $CuFe_2O_4/SnO_2$ powders.

3.2. Particle size and morphology

The presence of nanosized particles of $CuFe_2O_4$ and $CuFe_2O_4/SnO_2$ has been confirmed through TEM analysis. The nanocrystalline nature of $CuFe_2O_4$ with a particle size of approximately 10–20 nm and of SnO_2 coated $CuFe_2O_4$ with 20–30 nm are evident in Fig. 3(a and b), respectively.

Scanning electron micrographs recorded for $CuFe_2O_4$ and $CuFe_2O_4/SnO_2$ sintered at 1100 °C are given in Fig. 4(a and b), respectively. The presence of uniformly distributed spherical grains of independent nature with definite grain boundaries is a desirable morphological characteristic for battery electrodes [25]. Despite the high calcination temperature used in the synthesis, no obvious agglomeration is observed and is an indication of the size confinement of the individual particles.

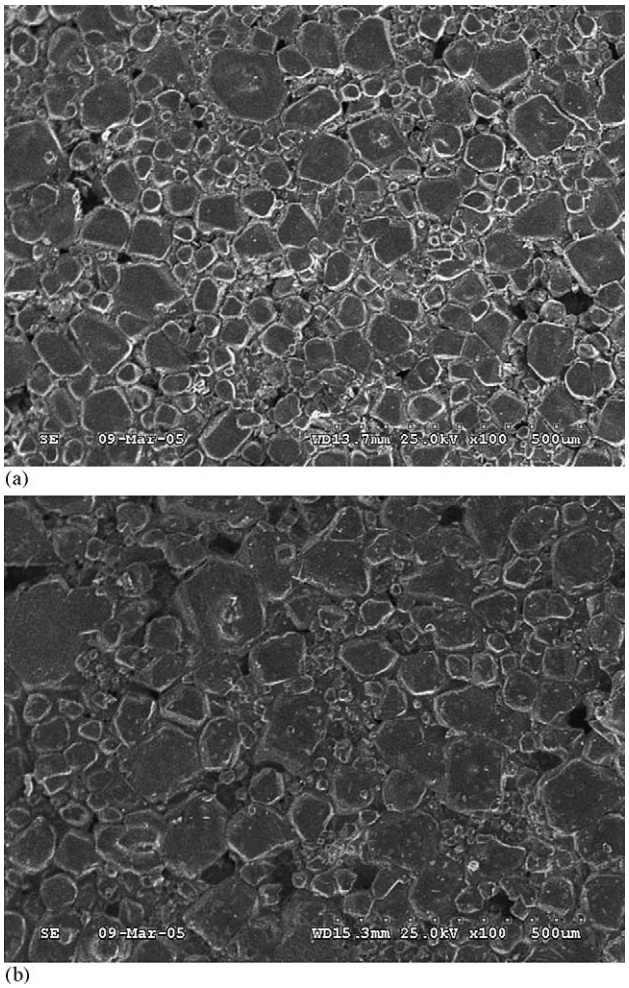

Fig. 4. SEM images of (a) $CuFe_2O_4$ and (b) $CuFe_2O_4$/10 wt.% SnO_2 powders.

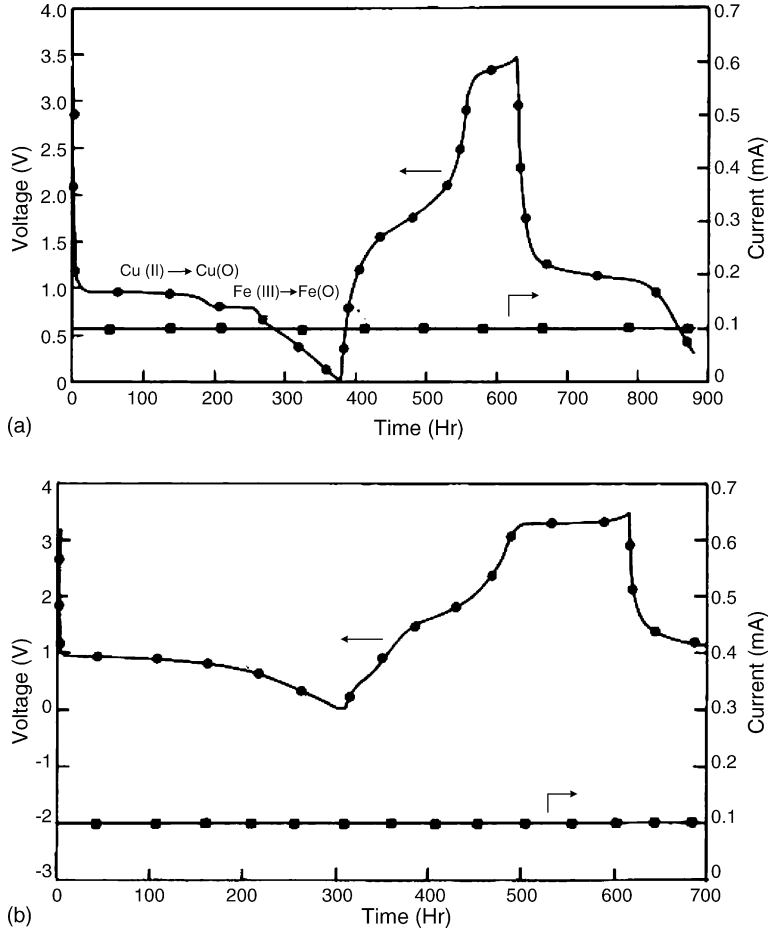

Fig. 5. Charge–discharge profiles exhibited by (a) $CuFe_2O_4$ and (b) $CuFe_2O_4/SnO_2$ anodes.

3.3. Charge–discharge behaviour

Charge–discharge profiles recorded for combustion-synthesized $CuFe_2O_4$ and SnO_2-doped $CuFe_2O_4$ anodes at a current density of $0.1\,mA\,cm^{-2}$ over the voltage region 3.5–0.1 V are presented in Fig. 5(a and b), respectively. The appearance of two potential plateaux around 0.9 and 0.75 V can be attributed to the corresponding reduction of Cu(II) to Cu(0) and Fe(III) to Fe(0) [15]. These findings are similar to those reported for $CoFe_2O_4$ anodes. Generally, two types of mechanisms are advanced for the decomposition of MFe_2O_4 anodes, namely:

displacive redox mechanism

$$MFe_2O_4 + 8Li^+ + 8e^- \leftrightarrow M + 2Fe + 4Li_2O \quad (1a)$$

$$4Li_2O + M + 2Fe \leftrightarrow MO + Fe_2O_3 + 8Li \quad (1b)$$

alloy-forming mechanism

$$MFe_2O_4 + 5Li^+ + 5e^- \leftrightarrow Li\text{–}M + 2FeO + 2Li_2O \quad (2)$$

The present set of $CuFe_2O_4$ and $CuFe_2O_4/SnO_2$ anodes are believed to follow the displacive redox mechanism. This is because the observed high specific capacity value of ~800 mAh g^{-1} can be correlated with the comparatively higher Li^+ uptake (~8 Li^+ per formula unit) and higher thermodynamic feasibility of the displacive redox mechanism. On the other hand, whereas the alloy-forming mechanism (Eq. (2)) would normally lead to an irreversible capacity loss, this is not observed with the present set of anodes. For example, it is quite evident from Fig. 5(a and b) that the second discharge capacity value is much closer to the initial one, particularly in the case of $CuFe_2O_4/SnO_2$. Therefore, it is clear that $CuFe_2O_4$ and the $CuFe_2O_4$/10 wt.% SnO_2 anodes follow the displacive redox mechanism, similar to that of transition metal oxide anodes [14–19]. The appearance of a slightly enhanced potential plateau around 1.2 V on the second cycle (Fig. 5(a and b)) of both of the ferrite anodes corresponds to the poorly crystalline/amorphous nature of the reduced products [18] obtained from Eq. (1). This provides further evidence that the chosen $CuFe_2O_4$ and SnO_2-doped $CuFe_2O_4$ anodes follow the displacive redox mechanism.

sThe high specific capacity values exhibited by both the ferrite anodes (>800 mAh g^{-1}) may be attributed to the electrochemically driven size confinement of the nanoelectrodes employed in the present study. Nanosize particle

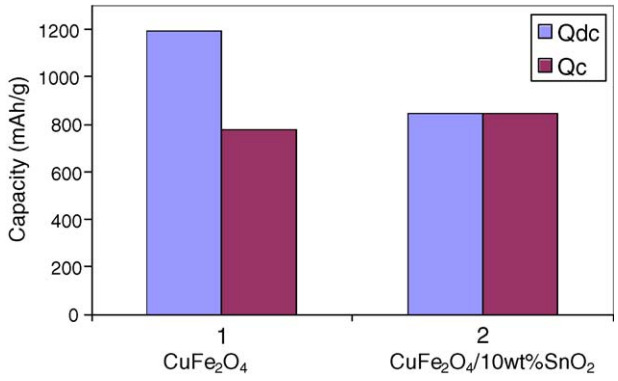

Fig. 6. Variation of discharge capacity (Q_{dc}) and charge capacity (Q_c) exhibited by (a) $CuFe_2O_4$ and (b) $CuFe_2O_4/SnO_2$ anodes.

characteristics of electrodes have been found to be effective in reducing the diffusion distance of lithium ions and in enhancing the diffusion kinetics [26]. As a result, the nano $CuFe_2O_4$ anode and $CuFe_2O_4/SnO_2$ nanocomposites have delivered an improved specific capacity of 1193 and 849 mAh g^{-1}, respectively. These values are almost three times higher than that of a carbon anode (372 mAh g^{-1}).

The SnO_2 (10 wt.%)-doped $CuFe_2O_4$ anode exhibits an excellent charging capacity of 845 mAh g^{-1} against a discharge capacity of 849 mAh g^{-1}, which is equivalent to a coulombic efficiency of 99.5% (Fig. 6). By contrast, the undoped $CuFe_2O_4$ anode delivers a charging capacity only of 779 mAh g^{-1} against 1193 mAh g^{-1} of initial discharge capacity, as evident from Fig. 6. Therefore, the coulombic efficiency of the $CuFe_2O_4$ anode is only 65%. Hence, a remarkable improvement in the capacity retention behaviour (Fig. 7) of copper ferrite has been made possible through SnO_2 doping. The dopant SnO_2 plays a vital role in enhancing the contact between the active material, binder, and the current-collector of the electrodes and thereby imparts better structural integrity and minimizes volume changes.

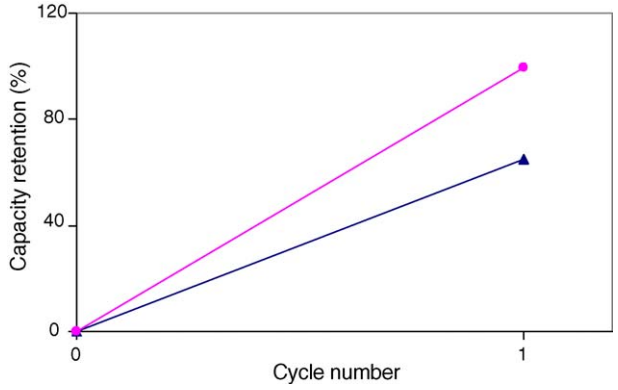

Fig. 7. Comparison of capacity retention of (▲) $CuFe_2O_4$ and (●) $CuFe_2O_4/SnO_2$ nanocompounds.

4. Conclusions

Nano $CuFe_2O_4$ and $CuFe_2O_4/SnO_2$ nanocomposites have been made by means of a urea–nitrate combustion method. The homogeneity and crystallinity of the synthesized powders are examined by X-ray diffraction analysis and the particle size (10–30 nm) by TEM analysis. On discharge at 0.1 mA cm^{-2}, the $CuFe_2O_4$ anode exhibits a capacity of 1193 mAh g^{-1} and the $CuFe_2O_4/SnO_2$ nanocomposite a capacity of 849 mAh g^{-1}. The coulombic efficiency of copper ferrite anodes is improved from 65 to 99.5% through SnO_2 doping. The present work is the very first of its kind to demonstrate the electrochemical behaviour of $CuFe_2O_4/SnO_2$ composites and the exploitation of SnO_2 doping for enhancing the capacity retention of in lithium batteries.

Acknowledgements

The authors deeply thank Prof. A. Gedanken, Bat-Ilan University, Israel, for provision of the TEM facility and Prof. A.K. Shukla, Director of, CECRI, for his kind assistance.

References

[1] P. Polzot, S. Laruella, S. Grugeon, L. Dupont, J.M. Tarascon, Nature 407 (2000) 496.
[2] C.R. Sides, C.R. Martin, Adv. Mater. 17 (2005) 125.
[3] M. Hibino, K. Abe, Masafumi, Mochizuki, M. Miyayama, J. Power Sources 126 (2004) 139.
[4] J. Xie, X.B. Zhao, G.S. Cao, Y.D. Zhong, M.J. Zhao, J.P. Tu, Electrochim. Acta 50 (2005) 1903.
[5] Y.-U. Kim, S.-I. Lee, C.K. Lee, H.-J. Sohn, J. Power Sources 141 (2005) 163.
[6] X.-Q. Cheng, P.-F. Shi, J. Alloys Compd. 391 (2005) 241.
[7] M.V. Reddy, C. Wannek, B. Pecquenard, J. Power Sources 119–121 (2003) 101.
[8] S.H. Choi, J.S. Kim, Y.S. Yoon, Electrochim. Acta 50 (2004) 545.
[9] Y. Idota, T. Kubota, A. Matsufuji, T. Miyasaka, Science 276 (1997) 1395.
[10] M. Nishijma, Y. Takeda, N. Imanishi, O. Yamamota, J. Solid State Chem. 113 (1994) 205.
[11] M.V.V.M. Satya Kishore, U.V. Varadaraju, B. Raveau, J. Solid State Chem. 77 (2004) 3981.
[12] N. Kalaiselvi, C.-H. Doh, C.-W. Park, S.-I. Moon, M.-S. Yun, Electrochem. Commun. 6 (2004) 1110.
[13] J.T. Son, Electrochem. Commun. 6 (2004) 990.
[14] Y.-Q. Chu, Z.-W. Fu, Q.-Z. Qin, Electrochim. Acta 49 (2004) 4915.
[15] X. Yang, X. Wang, Z. Zhang, J. Crystal Growth 277 (2005) 463.
[16] R. Alcántara, M. Jaraba, P. Lavela, J.L. Tirado, J.C. Jumas, J. Olivier-Fourcade, Electrochem. Commun. 5 (2003) 16.
[17] Y.-N. NuLi, Q.-Z. Qin, J. Power Sources 142 (2005) 292.
[18] Y.-N. NuLi, Y.-Q. Chu, Q.-Z. Qin, J. Electrochem. Soc. 151 (2004) A1077.
[19] N. Sharma, K.M. Shaju, G.V. Subba Rao, B.V.R. Chowdari, J. Power Sources 124 (2003) 204.
[20] H.-J. Ahn, H.-C. Choi, K.-W. Park, S.-B. Kim, Y.-E. Sung, J. Phys. Chem. B 108 (2004) 9815.

[21] J. Fan, T. Wang, C. Fu, B. Tu, Z. Jiang, D. Zhao, Adv. Mater. 16 (2004) 1432.
[22] Y. Wang, J.Y. Lee, B.-H. Chen, J. Electrochem. Soc. 151 (2004) A563.
[23] T. Prem Kumar, R. Ramesh, Y.Y. Lin, G.T.K.-Fey, Electrochem. Commun. 6 (2004) 520–525.
[24] R. Kalai Selvan, C.O. Augustin, L. John Berchmans, R. Saraswathi, Mater. Res. Bull. 38 (2003) 41.
[25] P. Kalyani, N. Kalaiselvi, N. Muniyandi, Mater. Chem. Phys. 77 (2003) 662.
[26] S. Panero, B. Scrosati, M. Wachtler, F. Croce, J. Power Sources 129 (2004) 90.